PNAS
www.pnas.org

Supplementary Information for

Metapopulation stability in branching river networks

Akira Terui*, Nobuo Ishiyama, Hirokazu Urabe, Satoru Ono, Jacques C. Finlay, Futoshi Nakamura

*Corresponding author

Email: hanabi0111@gmail.com

This PDF file includes:

Other supplementary materials for this manuscript include the following:

1. Statistical self-similarity of branching patterns

Statistical similarity can be assessed by comparing probability distributions. If two random variables, say X and Y, have the same probability distributions [i.e.,$f_X(x) = f_Y(x)$], then $X \overset{d}{=} Y$. However, it is also possible that apparently different variables become statistically similar after simple scaling. For example, the distributions of the rescaled random variables $X/E(X)$ and $Y/E(Y)$ might be the same random variable Z. In this case, the random variables X and Y are said to be statistically similar (1), and it suffices the following equation:

$$X \overset{d}{=} \left[\frac{E(X)}{E(Y)}\right] Y \tag{1.1}$$

Here we briefly describe that branching structure in our theoretical model possesses the above statistical self-similarity, whose recursive patterns are largely determined by branching probability P. To describe this, we introduce a concept of "generation" proceeding upstream from the river outlet. At each generation, each node in generation ω gives one or two nodes to the next upstream generation $\omega + 1$. Each node in generation ω has the distinct pathway of the same distance (i.e., ω) to the outlet. Generation is zero at the river outlet node.

Let X_ω be a random variable denoting the number of nodes in generation ω, and let $x_{i,\omega}$ be a random variable representing the number of "offspring (upstream)" nodes produced by a single "parental (downstream)" node. This means

$$X_\omega = \sum_{i=1}^{X_{\omega-1}} x_{i,\omega} \qquad \omega \in \{0, 1, 2, \ldots\} \tag{1.2}$$

Below, we refer to X_ω as the number of branches in generation ω since it is equivalent to the number of nodes in generation ω.

Now suppose that binary river networks are sufficiently large ($N \to \infty$). Because each parental node independently produces offspring node(s) [$Pr(x_{i,\omega} = 1) = 1 - P;\ Pr(x_{i,\omega} = 2) = P$], the expected values for $x_{i,\omega}$ and X_ω are

$$E(x_{i,\omega}) = \{2 \times P + 1 \times (1 - P)\} = P + 1 \tag{1.3a}$$

$$E(X_\omega) = (P + 1)^\omega \tag{1.3b}$$

This branching process of infinite river networks is relevant to the Galton-Watson branching process for the supercritical case, where the expected number of offspring m exceeds one (in our case $m = P + 1$). The theorem states that $X_\omega / E(X_\omega)$ converges with probability 1.0 to a limiting random variable W as $\omega \to \infty$ (2). Hence, with probability 1.0,

$$\frac{X_\omega}{(P+1)^\omega} \to W \qquad \omega \to \infty \tag{1.4}$$

Equation 1.4 implies that the probability distribution for the rescaled branch numbers obey

$$Pr\left(\frac{X_\omega}{m^\omega} \leq a\right) - Pr\left(\frac{X_k}{m^k} \leq a\right) \to 0 \qquad \omega, k \to \infty \tag{1.5}$$

where $m = P + 1$ and a is an arbitrary random variable. This convergence in probability distribution can be rewritten as

$$X_\omega \overset{d}{=} m^{\omega-k} X_k \qquad \omega \geq k;\ \omega, k \to \infty \tag{1.6}$$

Notice that the statistical property of X_ω is essentially defined by branching probability P. This demonstrates that the branching structure (measured as the number of branches in a given generation) has the form of statistical self-similarity in the sense defined by equation 1.1.

2. Derivation for the expected value of φ

The total number of within-branch combinations of nodes can be expressed as $\varphi = \sum {}_{n_j}C_2$ for branches with $n_j \geq 2$. The expected number of nodes (subpopulations) within those branches ($n_j \geq 2$), $E(n')$, is the expected value of a geometric distribution truncated at two:

$$E(n') = \sum_{n=2}^{\infty} \left[n \times \frac{P(1-P)^{n-1}}{1-P} \right] \quad (2.1)$$

In this equation, the denominator represents the probability of a branch having ≥ 2 nodes ($n_j \geq 2$), such that the cumulative mass function for the truncated geometric distribution (i.e., $\sum_{n=2}^{\infty} \frac{P(1-P)^{n-1}}{1-P}$) sums up to be unity. The above equation can be reexpressed as:

$$E(n') = \frac{1-P^2}{P(1-P)} \quad (2.2)$$

As the expected number of branches with $n_j \geq 2$ is $NP(1-P)$ [i.e., the number of branches in a network (NP) multiplied by the probability of a branch having ≥ 2 nodes ($1-P$)], the expected value of φ is:

$$E(\varphi) = NP(1-P) \times {}_{E(n')}C_2 = NP(1-P) \times \frac{[E(n') \times \{E(n')-1\}]}{2} \quad (2.3)$$

which yields $E(\varphi) = \frac{N}{2}\left(\frac{1-P^2}{P}\right)$.

3. Effects of unequal subpopulation abundances and CVs on metapopulation stability

Our theoretical model involves two simplified assumptions: equal temporal means and CVs of abundances for all subpopulations. We examined how these simplified assumptions influenced theoretical predictions of metapopulation stability using stochastic simulations.

We assumed an exponential decline in mean abundances of subpopulations with rank as $\mu_i = \mu_1 \exp[-b(i-1)]$, where μ_i is the temporal mean of *i*th subpopulation abundance and μ_1 is the temporal mean of the largest subpopulation. The parameter b determines the rate of decline in subpopulation abundance with increasing rank. That is, larger values of b indicate more unequal abundances of subpopulations. We also assumed the following mean-variance relationship of subpopulations (Taylor's power law): $\sigma_i^2 = c\mu_i^z$. Subpopulation CVs are constant across all subpopulations if the Taylor's exponent z equals two ($\sigma/\mu = c^{\frac{1}{2}}$). Otherwise, subpopulation CVs either increase ($z > 2$) or decrease ($z < 2$) with increasing mean abundance of subpopulation.

We generated random river networks as described in the main text and assigned subpopulation ID (i.e., abundance rank) randomly to each node. Metapopulation stability CV_m was then calculated based on the following formula.

$$CV_m = \frac{\sum_{i=1}^{N} \sigma_i^2 + 2\sum_{i=1}^{N-1}\sum_{j=i+1}^{N} Cov(x_i, x_j)}{\sum_{i=1}^{N} \mu_i}$$

We considered 54 combinations of parameters ($b = 0.01, 0.1$; $z = 1.5, 2.0, 2.5$; $\rho_{wb} = 0.1, 0.5, 0.9$; $\rho_{ab} = 0.1, 0.5, 0.9$). For simplicity, c and μ_1 were set as 1 and 100, respectively, for all simulations. Branching probability P and metapopulation size N varied as described in the main text. The R script was provided in Code S6.

The results were qualitatively similar. Branching complexity had stabilizing effects on metapopulations as long as within-branch synchrony exceeded among-branch synchrony (Figs. S3–8). In contrast, effects of metapopulation size greatly varied depending on parameter values (Figs. S9–14). Thus, our main conclusion based on the simplified model (equal mean abundances and CVs of subpopulations) may hold true in a variety of ecological contexts.

4. Individual-based simulation model

Model description

To investigate sensitivity of our theoretical predictions to realistic ecological processes, we developed an individual-based simulation model with discrete generations (3-5). In the model, we simulated subpopulation dynamics x_{ti} (generation *t* and patch *i*) in random river networks with explicit consideration of dispersal, reproduction and local/regional environmental stochasticity. Below, we explain details of our individual-based simulation model.

Dispersal – We assumed natal dispersal (i.e., disperse before reproduction), which is a common feature of riverine organisms (e.g., 6). Subpopulation size after natal dispersal, y_{ti}, was given by the following equation:

$$y_{ti} = x_{ti} + \sum_{j=1}^{N} I_j - M_i \quad (4.1)$$

I_j is the number of immigrants from patch *j* ($j \neq i$) to patch *i* and M_i is the number of migrants emigrating from patch *i* to other pathes. I_j and M_i were drawn as follows:

$$E(I_j) = x_{tj} \frac{p_s(1-p_s)^{d_{ij}}}{\zeta(d_{ij})} \quad (4.2a)$$

$$E(M_i) = x_{ti}(1-p_s) \quad (4.2b)$$

The parameter p_s dictates the probability of staying in patch *j* (i.e., $\text{dispersal rate} = 1 - p_s$), and the power d_{ij} is the network distance between patch *i* and *j* (measured as the number of habitat patches along the network). Dispersal probability for a given separation distance $[p_s(1-p_s)^{d_{ij}}]$ was devided by the number of subpopulation combinations with equal separation distance $\zeta(d_{ij})$ so that $\sum_{i=1}^{N} \frac{p_s(1-p_s)^{d_{ij}}}{\zeta(d_{ij})} = 1$ for large N. We used a discrete form of distance-dependent dispersal since our random river networks have discrete habitat patches. A continuous version of equation 4.2a is an exponential decay of dispersal probability, a common assumption made in metapopulation studies (e.g., 7). The immigration process described above is naturally downstream-biased as more connections exist in an upstream direction ["slow current" scenario *sensu* Fronhofer and Altermatt (3)], reflecting natural dispersal processes in real river networks.

Reproduction – We then simulated reproductive processes in local habitat patches using the logistic growth model provided by Beverton and Holt (8) (i.e., intraspecific competition occurs at the local subpopulation level).

$$E(x_{[t+1]i}) = y_{ti}\frac{g_{ti}}{1+ay_{ti}} \quad (4.4)$$

where $a = \frac{g_0-1}{K}$. K is the carrying capacity and g_0 represents the maximum per-capita population growth rate. Our model accounts for local, spatio-temporally uncorrelated enviromental stochasticity expressed as varition in population growth rate. For every patch and generation, g_{ti} was drawn from a log-normal distribution as: $\log g_{ti} \sim \text{Normal}(\log g_0, \sigma_g^2)$. The realized subpopulation size in the next generation was drawn from a Poisson distribution with a mean of $x_{[t+1]i}$ to represent local demographic stochasticity.

Regional catastrophic event – Finally, we assumed that metapopulations may experience regional declines at a certain rate (*e*) due to external, density-independent factors, such as watershed-wide floods or droughts. We considered two scenarios in which sensitivity to such external factors are either heterogeneous or homogenous among branches. In the heterogenous scenario, a simulated catastrophic event removed, on average, 40% of individuals from all patches simultaneously. We let removal rates vary randomly around the mean among branches (see Fig. 1 for definition of an individual branch) to account for substantial variation in disturbance regimes among branches, as widely observed in stream networks (9-11), and stream-specific life-history adaptation of subpopulations (12, 13) (see Discussion for further rational behind this assumption). In generations where regional catastrophic events occur, equation 4.4 becomes:

$$E(x_{[t+1]i}) = (1 - m_{k(i)})\left(y_{ti}\frac{g_{ti}}{1+ay_{ti}}\right) \quad (4.5)$$

$m_{k(i)}$ is the removal rate (patch *i* nested within branch *k*) drawn from a beta distribution: $m_k \sim \text{Beta}(0.8, 1.2)$, where $E(m_k) = 0.4$ and $Var(m_k) = 0.08$. This model structure allows us to account for spatial heterogeneity of sensitivity to a regional catastrophic event among

branches. In the homogeneous scenario, a simulated catastrophic event removed 40% of individuals from all patches with no spatial heterogeneity ($m_k = 0.4$ in equation 4.5). This scenario may represent human-altered landscapes, where stream-specific reponses are compromized due to, for example, fish stocking and/or flow regulations.

Numerical simulation

We chose 32 parameter combinations so as to represent metapopulation dynamics of ecologically distinct species (population growth rate $g_0 = 1.5, 3.0$; local environmental stochasticity $\sigma_g = 0.1, 0.5$; probability of staying $p_s = 0.9, 0.99$; occurrence rate of a regional catastrophic event $e = 0.1, 0.2$; heterogeneous or homogeneous removal rate m_k). In each parameter combination, we simulated 400 generations in 500 random river networks with varying branching probability *P* and metapopulation size *N*, both of which were randomly drawn from uniform distributions [$P \sim \mathrm{U}(0.1, 0.9)$; $N \sim \mathrm{U}(50, 150)$]. After discarding the first 100 generations as a burnin period, we estimated CVs of metapopulations ($\mathrm{CV_m}$) as: $\mathrm{CV_m} = \frac{SD(X_t)}{Mean(X_t)}$, where $X_t = \sum_1^N x_{ti}$. To examine if systematic heterogeneity of population synchrony emerges as a result of realistic ecological processes, we also estimated within-branch and among-branch population synchronies (measured as the Pearson's correlation coefficient) using the simulated subpopulation dynamics. We obtained median estimates of synchrony values for within-branch and among-branch combinations separately. For all parameter settings, all habitat patches were intialized with 100 individuals and carrying capacity *K* was set to be 100 individuals. The R scripts were provided in Code S7 and S8.

Among the resulting 16,000 metapopulation simulations, 22 metapopulations went extinct after 400 generations; these simulated metapopulations were discarded. In persistent metapopulations, a balance between within-branch and among-branch population synchronies were strongly influeced by regional catastrophic events (Fig. S15). In the presence of stream-specific responses to a regional catastrophic event, within-branch population synchrony generally exceeded among-branch population synchrony (compare red and gray dots in Fig. S15). Local environmental stochasticity (σ_g) and dispersal (p_s) also influenced within-branch and among-branch population synchronies; however, their effects were not as strong as regional catastrophic events and did not reverse the balace between within-branch and among-branch synchornies (compare panels in Fig. S15).

The resulting metapopulation dynamics were qualitatively similar to our analytical predictions. In ecological conditions where within-branch population synchrony clearly exceeded among-branch population synchrony, branching complexity consistently stabilized metapopulations (Fig. S16). The stabilizing effect of branching complexity diminished (or reversed in a few cases) as among-branch population synchrony became more similar to (or higher than) within-branch population synchrony (Fig. S16). As expected from the simplified theoretical models (see Fig. S2), metapopulation size effects were generally weak; the effects were detectable only when strong local environmental stochasticity lowered overall population synchrony ($\sigma_g = 0.5$; Fig. S17).

Collectively, these findings suggest that the functional relationship between metapopulation stability and branching complexity (or metapopulation size) was largely governed by the emergent balance of within-branch and among-branch population synchronies. Therefore, our conclusion derived from the simplified theoretical models is supported by detailed consideration of realistic ecological processes.

5. Study watershed and data selection of fish abundance data

Our study locations are designated as protected watersheds, and thus, have no major dams and fishery activities. Moreover, surrounding landscapes have little influence of human activities; forested area exceeded, on average, 86% of watershed area (Table S1). The only significant human influence is a well-documented artificial propagation program of masu salmon (*O. m. masou*) for a subset of watersheds.

We analyzed metapopulations of four fish species (*B. toni*, *O. m. masou*, *S. leucomaenis* and *T. hakonensis*) using the data from these watersheds. To exclude watersheds without sufficient data for our statistical model, we confined our analysis to those in which a focal fish species occurred ≥ 3 times at least at one of the sampling sites. Consequently, the number of watersheds analyzed varied from 16 to 31 depending on species. Other species were excluded from our analysis for either of the following reasons: (ⅰ) high risk of species misidentification or (ⅱ) small sample size (species excluded if ≤ 10 watersheds meet the above criterion).

6. Site-year specific detectability

Fish sampling was conducted with two-pass removal (each pass includes electrofishing and cast net sampling) at all sites. To estimate site-year specific detectability in our data, we constructed a multinomial detectability model. Let $n_{k,ti(j)}$ (site *j* nested within watershed *i* in year *t*) denote the number of fish captured in *k*th removal. We modeled the matrix of observed fish numbers $n_{k,ti(j)}$ as a multinomial distribution, $n_{k,ti(j)}|N_{ti(j)}, \boldsymbol{\pi} \sim \text{Multinomial}(N_{ti(j)}, \boldsymbol{\pi})$, conditional on the unknown number of fish $N_{ti(j)}$ and the conditional probabilities of capture $\boldsymbol{\pi}$ associated with the two-pass removal. We let $\theta_{ti(j)}$ represent the probability of capture during a single removal from the site in year *t*. Then $\pi_{k,ti(j)} = \theta_{ti(j)}\left(1-\theta_{ti(j)}\right)^{k-1}$ specifies the probability of capture of fish during the *k*th removal, given that they have not been captured in earlier removals. The parameter $\theta_{ti(j)}$ was assumed to be site-year specific: $\text{logit}(\theta_{ti(j)}) = \xi + \epsilon_{ti(j)}$. The parameter $\epsilon_{ti(j)}$ is the random variation among sites and years (thus, observer-specific detection errors were also involved in this parameter) and was normally distributed as $\epsilon_{ti(j)} \sim \text{Normal}(0, \sigma_\epsilon^2)$. The average probability of capture with the two-pass removal across sites and years (γ) was given by $\gamma = \sum_k \delta(1-\delta)^{k-1}\ k \in \{1, 2\}$, where $\text{logit}(\delta) = \xi$. We assumed that the unknown number of fish $N_{ti(j)}$ follows an overdispersed-Poisson distribution as:

$$N_{ti(j)} \sim \text{Poisson}(\kappa_{ti(j)})$$
$$\log \kappa_{ti(j)} \sim \text{Normal}(\log \kappa_{mean}, \sigma_\kappa^2)$$

The parameters κ_{mean} and σ_κ represent the expected mean and the overdispersion parameter governing normally-distributed errors, respectively.

The model was fitted to the data with JAGS as in the main text. Vague priors were assigned to the parameters: i.e., normal distributions for $\log \kappa_{mean}$ and ξ (mean = 0, variance = 10^3) and truncated normal distributions for σ_ϵ and σ_κ (mean = 0, variance = 10^3, range = 0–30). Three MCMC chains were run to calculate poterior probabilities. Estimated parameters were summarized in Table S4.

7. Estimation of elevation, watershed land cover and weir density

Using QGIS ver 2.12.3, we estimated elevation, watershed land cover (measured as % forest area) and weir density as follows. Elevation averaged for each watershed was estimated based on the digital elevation map of 90-m resolution. We estimated % forest area in each watershed as a proxy for watershed land cover (the rest of area is attributable to human-altered land such as dairy) using the Advanced Land Observing Satellite (ALOS; ©JAXA) images from 2006 to 2011 (resolution 100 × 100 m). The ALOS images are available at http://www.eorc.jaxa.jp/ALOS/en/index.htm. Weir distribution data across Hokkaido were compiled by Hokkaido Institute of Environmental Sciences based on information from Department of Fisheries and Forestry, Hokkaido Government and National Land numerical information, and the Ministry of Land, Infrastructure, Transport and Tourism of Japan.

We did not include elevation, watershed land cover and weir density in the regression model explaining metapopulation stability because these variables were less informative and/or risked influences of multicollinearity. Elevation was not considered as it was correlated with precipitation (Pearson's $r = 0.68$, $p < 0.01$) and may be substituted by the variable. Watershed land cover (% forest area) and weir density (number of weirs per watershed area) were not included for the following reasons: (ⅰ) these variables were clearly correlated with multiple explanatory variables, so including them in a regression model risked influences of multicollinearity; (ⅱ) there was very minor variation in land cover (Table S1); (ⅲ) majority of weirs occurred in tiny headwater streams (<1 km^2 watershed area) and thus have little influence on watershed-scale connectivity (14); (ⅳ) these two variables were not correlated with the detrended CV (Pearson's $|r| < 0.04$, $p > 0.74$). See Table S5 for a full correlation matrix among potential explanatory variables.

References

1. Peckham SD & Gupta VK (1999) A reformulation of Horton's laws for large river networks in terms of statistical self‐similarity. *Water Resources Research* 35:2763-2777.
2. Harris TE (2002) *The theory of branching processes* (Courier Corporation).
3. Fronhofer EA & Altermatt F (2017) Classical metapopulation dynamics and eco-evolutionary feedbacks in dendritic networks. *Ecography* 40:1455-1466.
4. Fronhofer EA, Kubisch A, Hilker FM, Hovestadt T, & Poethke HJ (2012) Why are metapopulations so rare? *Ecology* 93:1967-1978.
5. Fronhofer EA, Stelz JM, Lutz E, Poethke HJ, & Bonte D (2014) Spatially correlated extinctions select for less emigration but larger dispersal distances in the spider mite *Tetranychus urticae*. *Evolution* 68:1838-1844.
6. Macneale KH, Peckarsky BL, & Likens GE (2005) Stable isotopes identify dispersal patterns of stonefly populations living along stream corridors. *Freshwater Biology* 50:1117-1130.
7. Hanski I (1999) *Metapopulation ecology* (Oxford University Press, Oxford).
8. Beverton RJ & Holt SJ (1957) *On the dynamics of exploited fish populations.* (Chapman and Hall, London).
9. Nakamura F, Swanson FJ, & Wondzell SM (2000) Disturbance regimes of stream and riparian systems-a disturbance-cascade perspective. *Hydrological Processes* 14:2849-2860.
10. Benda L, *et al.* (2004) The network dynamics hypothesis: how channel networks structure riverine habitats. *Bioscience* 54:413-427.
11. Moore JW, *et al.* (2015) Emergent stability in a large, free‐flowing watershed. *Ecology* 96:340-347.
12. Schindler DE, *et al.* (2010) Population diversity and the portfolio effect in an exploited species. *Nature* 465:609-612.
13. Moore JW & Schindler DE (2010) Spawning salmon and the phenology of emergence in stream insects. *Proceedings of the Royal Society B: Biological Sciences* 277:1695-1703.
14. Cote D, Kehler DG, Bourne C, & Wiersma YF (2009) A new measure of longitudinal connectivity for stream networks. *Landscape Ecology* 24:101-113.
15. Miyazaki Y, *et al.* (2011) Ecological evaluation of the conservation of fish fauna in the Shubuto River system, southwestern Hokkaido. *Japanese Journal of Conservation Ecology* 16:213-219.

Table S1 Summary of watershed characteristics

Variable	Mean (SD)	Unit
Branching probability	0.5 (0.1)	km^{-1}
Watershed area	88.9 (83.0)	km^2
Average elevation	351.5 (152.0)	m
Precipitation[a]	1565.6 (306.1)	mm
Temperature[b]	6.1 (1.3)	℃
Number of hatchery fish[c]	3417.6 (3826.7)	10^3 fish
% forest area	86.8 (17.0)	%
Weir density	0.3 (0.4)	km^{-2}

[a] Annual cumulative precipitation

[b] Annual mean air temperature

[c] Cumulative number of harchery fish (*Oncorhynchus masou masou*) released since 1955

Table S2 Data availability table. Numbers in cells denote the number of sites surveyed in each year. Numbers in parentheses indicates the same statistic, but the sites in which reliable data of *Tribolodon hakonensis* are available (some data unavailable due to incomplete species identification).

Watershed	Year																	
	99	00	01	02	03	04	05	06	07	08	09	10	11	12	13	14	15	16
Atsuta	5	5	4	5	5	4	4	3	4	5	4	4	4	5	4	5	4	4
Chihase	0	0	0	2	0	0	0	2	0	2	0	2	0	0	0	0	2	0
Furuu	5	0	0	0	0	5	0	5	0	5	0	5	0	5	4	0	0	4
Futoro	0	0	0	3	0	0	0	3	0	3	0	3	0	3	0	0	2	0
Haraki	0	0	0	2	0	0	2	0	2	0	1	0	2	0	0	2	0	0
Hidakahorobetsu	4	0	0	4	0	0	0	3	0	3	0	3	0	3	0	0	3	0
Hime	0	0	0	3	0	0	3	0	3	0	3	0	3	0	3	0	0	3
Horonai	0	0	2	0	0	2	0	2	0	2	0	2	0	2	0	0	2	0
Ishizaki	4	0	0	0	4	0	0	0	4	0	4	1	4	0	0	0	2	0
Kenichi	5	5	5	5 (2)	5	4	5 (3)	5	5 (2)	5	5	5 (3)	5	5 (3)	0	4	0	0
Kokamotsu	3	0	0	0	2	0	0	3	0	3	0	3	0	3	0	0	1	0
Masuhoro	3	0	0	3	0	0	3	0	3	0	3	0	3	0	3	0	0	3
Mogusa	0	3	0	0	0	2	0	2	0	2	0	2	0	2	1	0	0	1
Nikanbetsu	5	5	5	5	0	5	5	4	5	5	5	5	5	5	5	5	5	5
Nishibetsu	0	5	0	0	0	3	0	5	0	5	0	5	0	5	0	5	0	0
Nobusha	3	0	3	0	0	0	0	3	0	3	0	3	0	3	0	0	2	0
Okushibetsu	0	3	0	0	0	3	0	3	0	3	0	3	0	2	0	0	3	0
Ookamotsu	3	3	3	3	3	3	3	3	3	3	3	3	3	3	3	3	0	2
Oyobe	0	3	0	0	0	0	3 (0)	0	3 (0)	0	3	0	3	0	0	3	0	0

Table S2 Continued

Watershed	Year																	
	99	00	01	02	03	04	05	06	07	08	09	10	11	12	13	14	15	16
Shakotan	5 (3)	5	5	5	5	5	5 (4)	5	5	5	5	5	5	4	5	5 (4)	5	5
Shimonaefutoro	3	3 (2)	3	3	3 (2)	3	3 (2)	3	3	3	3	3	3	3	3	3	3	3
Shiotomari	0	0	3	0	0	0	3	0	3	0	3	0	3	0	0	3	0	0
Shokanbetsu	1	3	3	3	3	3	3	3	3	3	3	3	3	3	3	0	0	3
Sukki	0	0	2	0	2	0	2	2	0	2	3	3	0	3	0	2	0	0
Tomari	0	3	0	0	0	0	3	0	3	0	2	0	3	0	0	3	0	0
Toppu	0	0	3	0	0	0	0	3	0	3	0	3	0	3	0	0	3	0
Toshibetsu	5	0	0	0	0	0	0	0	3	0	4	0	3	0	4	0	0	3
Usubetsu	0	3	0	0	0	0	3	0	3	0	3	0	3	0	3	0	0	3
Utabetsu	0	0	4	0	0	0	4	0	4	0	4	0	4	0	4	0	0	4
Yamubetsu	0	3	0	0	3	0	3	0	3	0	3	0	3	0	3	0	0	3
Yobetsu	0	0	2	0	0	0	2	0	2	0	2	0	2	0	0	2	0	0

Table S3 Ecological traits of fish species studied

Family	Species	Migration type[a]	Vertical habitat	Velocity preference[b]
Balitoridae	*Barbatula toni*	PF	Bottom	Semi-lentic
Cyprinidae	*Tribolodon hakonensis*	PF/A	Middle layer	Semi-lentic
Salmonidae	*Oncorhynchus masou masou*	PF/A	Middle layer	Lotic
	Salvelinus leucomaenis	PF/A	Middle layer	Lotic

[a] PF, primary freshwater; A, Anadromous; P/A, partially anadromous (i.e., some individuals migrate to the sea)

[b] Classified based on Miyazaki *et al.* (15)

Table S4 Estimation of site-year specific detectability.

Parameter	Species	Median	95% CI[a]
Average detectability γ	*B. toni*	0.73	0.63–0.80
	T. hakonensis	0.92	0.83–0.95
	O. m. masou	0.90	0.88–0.91
	S. leucomaenis	0.90	0.86–0.92
Site-year variation of detectability σ_{ε}[b]	*B. toni*	0.95	0.70–1.28
	T. hakonensis	0.64	0.44–0.93
	O. m. masou	0.99	0.90–1.08
	S. leucomaenis	0.82	0.66–1.02

[a] 95% CI, 95% credible interval

[b] Estimated in a logit-scale

Table S5 Correlation matrix (Pearson's *r*) of watershed characteristics. Significant correlations ($p < 0.05$) are shown in bold.

Variable	BP	WA	Elev	Prec	Temp	Hatchery	Forest	Weir
BP		−0.08	**0.36**	0.24	−0.14	0.16	**0.41**	0.00
WA			−0.24	**−0.37**	−0.30	**0.72**	**−0.61**	−0.16
Elev				**0.68**	−0.17	−0.04	**0.57**	−0.00
Prec					**0.37**	−0.04	**0.70**	**0.36**
Temp						−0.14	**0.40**	**0.52**
Hatchery							−0.33	−0.10
Forest								**0.40**
Weir								

Note: BP, branching probability; WA, watershed area; Elev, average elevation; Prec, cumulative precipitation (mm); Temp, mean air temperature (℃); Hatchery, number of hatchery fish released; Forest, % forest area; Weir, weir density (km^{-2})

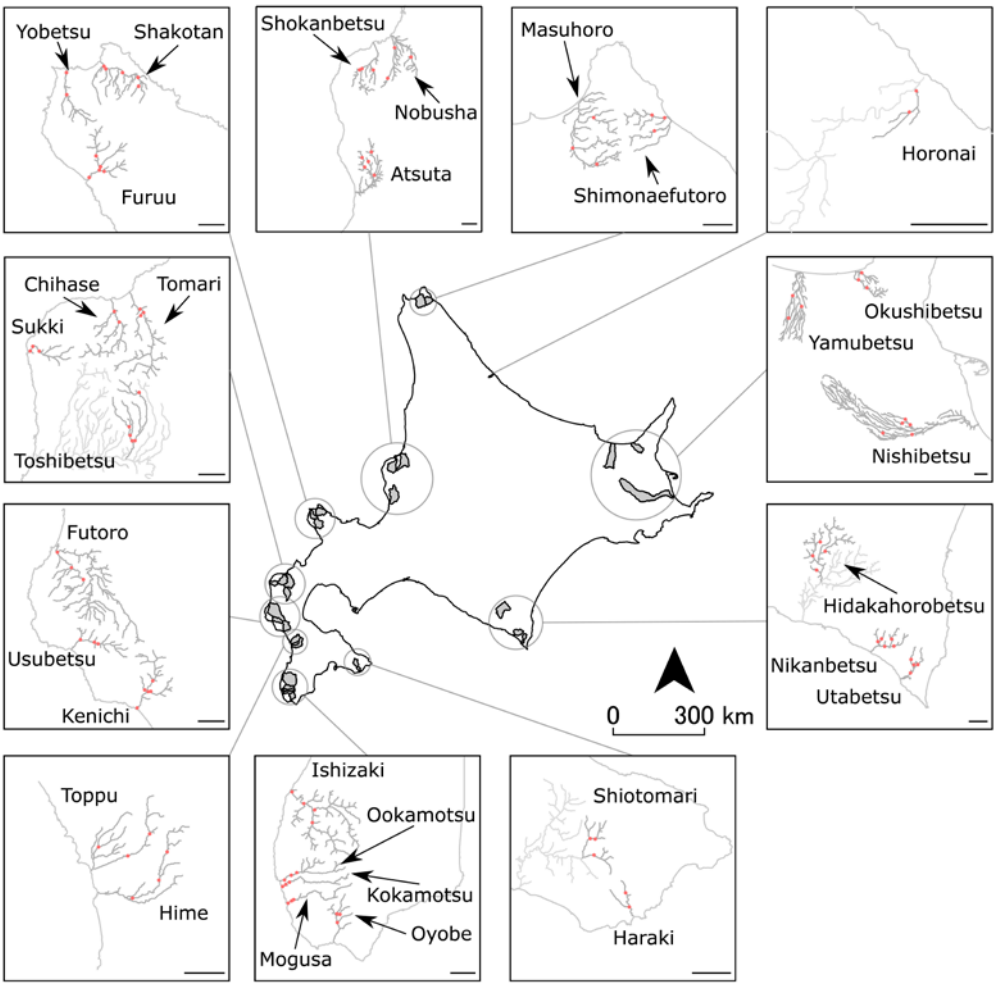

Figure S1 Rescaled map of study watersheds. In each panel, red dots indicate sampling sites, and scale bars are 5 km. River lines shown in light-gray indicate subwatersheds with no sampling sites (Hidakahorobetsu, Horonai, Shiotomari, Toshibetsu).

Figure S2 Theoretical predictions for relationships of metapopulation size N (expressed as the number of subpopulations) and stability when we assumed equal abundances and CVs for all subpopulations. Different panels denote differential combinations of within-branch (ρ_{wb}) and among-branch population synchronies (ρ_{ab}) [$\rho_{wb} = \rho_{ab}$ (a, e, i); $\rho_{wb} > \rho_{ab}$ (d, g, h); $\rho_{wb} < \rho_{ab}$ (b, c, f)]. Lower CVs indicate greater temporal stability of metapopulations in branching networks. Lines are analytical predictions of metapopulation stability and different line types denote predictions with differential branching probabilities (solid, P = 0.1; broken, 0.5; broken-dot, 0.9). Dots are the results of stochastic simulations and are colored in proportion to branching probability P (range: 0.1–0.9; from blue to ivory). CV_p was set to be 1 for simplicity (see equation 2).

Figure S3 Theoretical predictions for relationships of branching complexity and metapopulation stability. Different panels denote differential combinations of within-branch (ρ_{wb}) and among-branch population synchronies (ρ_{ab}) [(a, e, i): $\rho_{wb} = \rho_{ab}$; (d, g, h): $\rho_{wb} > \rho_{ab}$; (b, c, f): $\rho_{wb} < \rho_{ab}$]. Lower CVs indicate greater temporal stability of metapopulations in branching networks. Dots are colored in proportion to metapopulation size *N* (range: 50–150; from red to ivory). Parameters that determine a rank-abundance curve (*b*) and mean-variance relationship (*z*) of subpopulations were as follows: $b = 0.01$, $z = 1.5$.

Figure S4 Theoretical predictions for relationships of branching complexity and metapopulation stability. Different panels denote differential combinations of within-branch (ρ_{wb}) and among-branch population synchronies (ρ_{ab}) [(a, e, i): $\rho_{wb} = \rho_{ab}$; (d, g, h): $\rho_{wb} > \rho_{ab}$; (b, c, f): $\rho_{wb} < \rho_{ab}$]. Lower CVs indicate greater temporal stability of metapopulations in branching networks. Dots are colored in proportion to metapopulation size *N* (range: 50–150; from red to ivory). Parameters that determine a rank-abundance curve (*b*) and mean-variance relationship (*z*) of subpopulations were as follows: $b = 0.01$, $z = 2.0$.

Figure S5 Theoretical predictions for relationships of branching complexity and metapopulation stability. Different panels denote differential combinations of within-branch (ρ_{wb}) and among-branch population synchronies (ρ_{ab}) [(a, e, i): $\rho_{wb} = \rho_{ab}$; (d, g, h): $\rho_{wb} > \rho_{ab}$; (b, c, f): $\rho_{wb} < \rho_{ab}$]. Lower CVs indicate greater temporal stability of metapopulations in branching networks. Dots are colored in proportion to metapopulation size *N* (range: 50–150; from red to ivory). Parameters that determine a rank-abundance curve (*b*) and mean-variance relationship (*z*) of subpopulations were as follows: $b = 0.01$, $z = 2.5$.

Figure S6 Theoretical predictions for relationships of branching complexity and metapopulation stability. Different panels denote differential combinations of within-branch (ρ_{wb}) and among-branch population synchronies (ρ_{ab}) [(a, e, i): $\rho_{wb} = \rho_{ab}$; (d, g, h): $\rho_{wb} > \rho_{ab}$; (b, c, f): $\rho_{wb} < \rho_{ab}$]. Lower CVs indicate greater temporal stability of metapopulations in branching networks. Dots are colored in proportion to metapopulation size *N* (range: 50–150; from red to ivory). Parameters that determine a rank-abundance curve (*b*) and mean-variance relationship (*z*) of subpopulations were as follows: $b = 0.1$, $z = 1.5$.

Figure S7 Theoretical predictions for relationships of branching complexity and metapopulation stability. Different panels denote differential combinations of within-branch (ρ_{wb}) and among-branch population synchronies (ρ_{ab}) [(a, e, i): $\rho_{wb} = \rho_{ab}$; (d, g, h): $\rho_{wb} > \rho_{ab}$; (b, c, f): $\rho_{wb} < \rho_{ab}$]. Lower CVs indicate greater temporal stability of metapopulations in branching networks. Dots are colored in proportion to metapopulation size *N* (range: 50–150; from red to ivory). Parameters that determine a rank-abundance curve (*b*) and mean-variance relationship (*z*) of subpopulations were as follows: $b = 0.1$, $z = 2.0$.

Figure S8 Theoretical predictions for relationships of branching complexity and metapopulation stability. Different panels denote differential combinations of within-branch (ρ_{wb}) and among-branch population synchronies (ρ_{ab}) [(a, e, i): $\rho_{wb} = \rho_{ab}$; (d, g, h): $\rho_{wb} > \rho_{ab}$; (b, c, f): $\rho_{wb} < \rho_{ab}$]. Lower CVs indicate greater temporal stability of metapopulations in branching networks. Dots are colored in proportion to metapopulation size *N* (range: 50–150; from red to ivory). Parameters that determine a rank-abundance curve (*b*) and mean-variance relationship (*z*) of subpopulations were as follows: $b = 0.1$, $z = 2.5$.

Figure S9 Theoretical predictions for relationships of metapopulation size and stability. Different panels denote differential combinations of within-branch (ρ_{wb}) and among-branch population synchronies (ρ_{ab}) [(a, e, i): $\rho_{wb} = \rho_{ab}$; (d, g, h): $\rho_{wb} > \rho_{ab}$; (b, c, f): $\rho_{wb} < \rho_{ab}$]. Lower CVs indicate greater temporal stability of metapopulations in branching networks. Dots are colored in proportion to branching probability *P* (range: 0.1–0.9; from blue to ivory). Parameters that determine a rank-abundance curve (*b*) and mean-variance relationship (*z*) of subpopulations were as follows: $b = 0.01$, $z = 1.5$.

Figure S10 Theoretical predictions for relationships of metapopulation size and stability. Different panels denote differential combinations of within-branch (ρ_{wb}) and among-branch population synchronies (ρ_{ab}) [(a, e, i): $\rho_{wb} = \rho_{ab}$; (d, g, h): $\rho_{wb} > \rho_{ab}$; (b, c, f): $\rho_{wb} < \rho_{ab}$]. Lower CVs indicate greater temporal stability of metapopulations in branching networks. Dots are colored in proportion to branching probability *P* (range: 0.1–0.9; from blue to ivory). Parameters that determine a rank-abundance curve (*b*) and mean-variance relationship (*z*) of subpopulations were as follows: $b = 0.01$, $z = 2.0$.

Figure S11 Theoretical predictions for relationships of metapopulation size and stability. Different panels denote differential combinations of within-branch (ρ_{wb}) and among-branch population synchronies (ρ_{ab}) [(a, e, i): $\rho_{wb} = \rho_{ab}$; (d, g, h): $\rho_{wb} > \rho_{ab}$; (b, c, f): $\rho_{wb} < \rho_{ab}$]. Lower CVs indicate greater temporal stability of metapopulations in branching networks. Dots are colored in proportion to branching probability *P* (range: 0.1–0.9; from blue to ivory). Parameters that determine a rank-abundance curve (*b*) and mean-variance relationship (*z*) of subpopulations were as follows: $b = 0.01$, $z = 2.5$.

Figure S12 Theoretical predictions for relationships of metapopulation size and stability. Different panels denote differential combinations of within-branch (ρ_{wb}) and among-branch population synchronies (ρ_{ab}) [(a, e, i): $\rho_{wb} = \rho_{ab}$; (d, g, h): $\rho_{wb} > \rho_{ab}$; (b, c, f): $\rho_{wb} < \rho_{ab}$]. Lower CVs indicate greater temporal stability of metapopulations in branching networks. Dots are colored in proportion to branching probability *P* (range: 0.1–0.9; from blue to ivory). Parameters that determine a rank-abundance curve (*b*) and mean-variance relationship (*z*) of subpopulations were as follows: $b = 0.1$, $z = 1.5$.

Figure S13 Theoretical predictions for relationships of metapopulation size and stability. Different panels denote differential combinations of within-branch (ρ_{wb}) and among-branch population synchronies (ρ_{ab}) [(a, e, i): $\rho_{wb} = \rho_{ab}$; (d, g, h): $\rho_{wb} > \rho_{ab}$; (b, c, f): $\rho_{wb} < \rho_{ab}$]. Lower CVs indicate greater temporal stability of metapopulations in branching networks. Dots are colored in proportion to branching probability *P* (range: 0.1–0.9; from blue to ivory). Parameters that determine a rank-abundance curve (*b*) and mean-variance relationship (*z*) of subpopulations were as follows: $b = 0.1$, $z = 2.0$.

Figure S14 Theoretical predictions for relationships of metapopulation size and stability. Different panels denote differential combinations of within-branch (ρ_{wb}) and among-branch population synchronies (ρ_{ab}) [(a, e, i): $\rho_{wb} = \rho_{ab}$; (d, g, h): $\rho_{wb} > \rho_{ab}$; (b, c, f): $\rho_{wb} < \rho_{ab}$]. Lower CVs indicate greater temporal stability of metapopulations in branching networks. Dots are colored in proportion to branching probability *P* (range: 0.1–0.9; from blue to ivory). Parameters that determine a rank-abundance curve (*b*) and mean-variance relationship (*z*) of subpopulations were as follows: $b = 0.1$, $z = 2.5$.

Figure S15 Comparisons of within-branch and among-branch population synchronies in simulated metapopulations (i.e., individual-based simulation model). Dots are individual metapopulation replicates. Different panels represent the relationships derived from different ecological parameter combinations (g_0: maximum per-capita population growth rate, σ_g: local environmental stochasticity, p_s: probability of staying in the home patch, *e*: occurrence rate of a regional catastrophic event), and parameter values are shown on the top of each panel. Red and gray dots represent scenarios with heterogeneous and homogeneous stream responses to a regional catastrophic event, respectively. Note that dispersal rate can be expressed as $1 - p_s$. Broken lines are a 1:1 relationship, and simulated metapopulations (dots) above this line have greater within-branch population synchrony.

Figure S16 Relationships of branching complexity and metapopulation stability predicted from the individual-based simulation model. Dots are individual metapopulation replicates. Different panels represent the relationships drawn from different ecological parameter combinations (g_0: maximum per-capita population growth rate, σ_g: local environmental stochasticity, p_s: probability of staying in the home patch, *e*: occurrence rate of a regional catastrophic event), and parameter values are shown on the top of each panel. Red and gray dots represent scenarios with heterogeneous and homogeneous stream responses to a regional catastrophic event, respectively. Note that dispersal rate can be expressed as $1 - p_s$. Lines are predicted values from simple linear regressions of log CV and branching probability, and numbers on the topright of each panel represent standardized regression coefficients.

Figure S17 Relationships of metapopulation size and stability predicted from the individual-based simulation model. Dots are individual metapopulation replicates. Different panels represent the relationships drawn from different ecological parameter combinations (g_0: maximum per-capita population growth rate, σ_g: local environmental stochasticity, p_s: probability of staying in the home patch, *e*: occurrence rate of a regional catastrophic event), and parameter values are shown on the top of each panel. Blue and gray dots represent scenarios with heterogeneous and homogeneous stream responses to a regional catastrophic event, respectively. Note that dispersal rate can be expressed as $1 - p_s$. Lines are predicted values from simple linear regressions of log CV and metapopulation size, and numbers on the topright of each panel represent standardized regression coefficients.

Figure S18 Estimated metapopulation trends of *Barbatula toni.* Names on the top of each panel refer to watershed ID. Lines are median estimates. Shades represent 25% and 75% percentiles of posterior distributions.

Figure S19 Estimated metapopulation trends of *Tribolodon hakonensis*. Names on the top of each panel refer to watershed ID. Lines are median estimates. Shades represent 25% and 75% percentiles of posterior distributions.

Figure S20 Estimated metapopulation trends of *Oncorhynchus masou masou.* Names on the top of each panel refer to watershed ID. Lines are median estimates. Shades represent 25% and 75% percentiles of posterior distributions.

Figure S21 Estimated metapopulation trends of *Salvelinus leucomaenis.* Names on the top of each panel refer to watershed ID. Lines are median estimates. Shades represent 25% and 75% percentiles of posterior distributions.

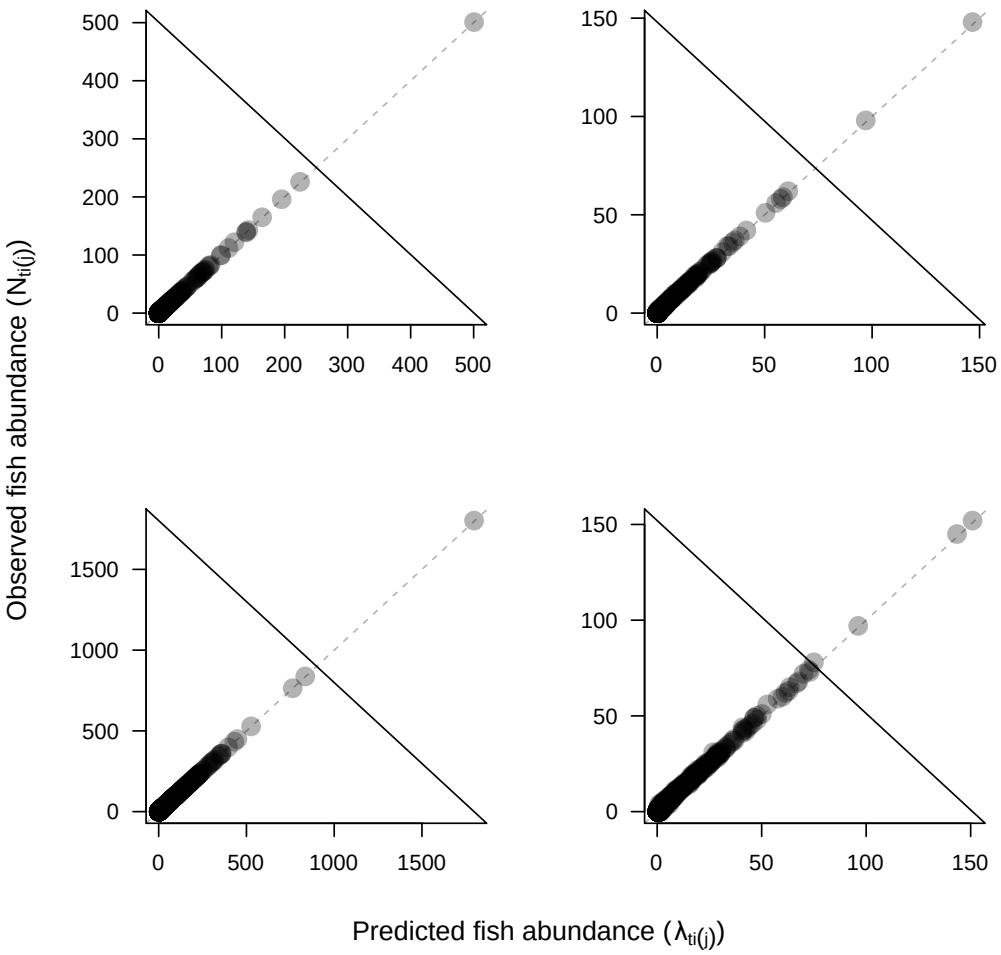

Figure S22 Comparisons of observed and predicted fish abundance at the site scale. Predicted fish abundance is the predicted values from the Bayesian state-space models ($\lambda_{ti(j)}$). Broken lines denote a 1:1 relationship. The Bayesian state-space models accurately predicted the observed fish abundance of four study species.